CrossMark

JfM PAPERS

Downscale energy fluxes in scale-invariant oceanic internal wave turbulence

Giovanni Dematteis[1],† and Yuri V. Lvov[1]

[1]Department of Mathematical Sciences, Rensselaer Polytechnic Institute, 110 8th St, Troy, NY 12180, USA

We analyse analytically and numerically the scale-invariant stationary solution to the internal-wave kinetic equation. Our analysis of the resonant energy transfers shows that the leading-order contributions are given (i) by triads with extreme scale separation and (ii) by triads of waves that are quasi-collinear in the horizontal plane. The contributions from other types of triads is found to be subleading. We use the modified scale-invariant limit of the Garrett and Munk spectrum of internal waves to calculate the magnitude of the energy flux towards high wavenumbers in both the vertical and the horizontal directions. Our results compare favourably with the finescale parametrization of ocean mixing that was proposed in Polzin *et al.* (*J. Phys. Oceanogr.*, vol. 25, issue 3, 1995, pp. 306–328).

1. Introduction

Internal waves are the gravity waves that oscillate in the bulk of the stratified ocean due to the modulation of surfaces of constant density. Internal waves are ubiquitous in the ocean, contain a large amount of energy and affect significantly the processes involved in water mixing and transport. Understanding the role played by internal gravity waves in the energy budget of the oceans represents a major challenge in physical oceanography, intimately related to the quantification of ocean mixing (Ferrari & Wunsch 2008; Polzin *et al.* 2014). Internal waves constitute a highly complex problem, involving scales from few metres to hundreds of kilometres, and periods ranging from a few minutes up to days. The processes that supply energy to and remove energy from internal waves include interactions with surface gravity waves, mesoscale eddies, scattering of the tidal flow from the bottom topography, overturning of wave fronts and wave breaking. These pumping and damping processes are characterized by vastly different spatial and temporal scales. Despite this enormous complexity, the spectral energy density of internal waves is thought to be pretty universal, and is given by what is now called the Garrett and Munk spectrum of

† Email address for correspondence: dematg@rpi.edu

internal waves. First proposed in 1972 (Garrett & Munk 1972), then subject to subsequent revisions (Garrett & Munk 1975; Cairns & Williams 1976; Garrett & Munk 1979), the Garrett and Munk spectrum (GM, from now on referring to the 1976 version) has since become the accepted default choice to quantify the oceanic internal wave field. Since then substantial deviations, both seasonal and regional, were documented (notably near boundaries (Wunsch & Webb 1979; Polzin 2004; Polzin & Lvov 2011), and at the equator (Eriksen 1985)). Nonetheless, the GM spectrum has survived to our day as the standard for intercomparison of different data sets, to the amazement of Chris Garrett and Walter Munk themselves (von Storch & Hasselmann 2010), providing the baseline for generalizations that try to account for the observed variability (Polzin & Lvov 2011).

The spectral energy fluxes in the oceanic internal wave field have been a subject of intense investigation in the last four decades (Olbers 1973; McComas & Bretherton 1977; Müller *et al.* 1986; Polzin, Toole & Schmitt 1995). Understanding these energy fluxes is crucial for climate modelling and predictions, since internal waves are not resolved in global circulation models (GCM) and they are replaced by simple phenomenological formulas (MacKinnon *et al.* 2017). One of such broadly used expressions is the finescale parametrization formula derived in Polzin *et al.* (1995).

In this paper, we use the wave-turbulence theory for internal gravity waves developed in Lvov & Tabak (2001), Lvov & Tabak (2004), Lvov *et al.* (2010) and Lvov & Yokoyama (2009) and reviewed in Polzin & Lvov (2011) to analyse these energy fluxes towards high wavenumbers. We assume that the spectral energy density of internal waves is given by a simple scale-invariant solution, that was found in Lvov *et al.* (2010), (hereafter, the convergent stationary solution of the internal-wave kinetic equation, (3.9) in the body of the paper). Interestingly, this scale-invariant spectrum is close to the scale invariant limit of the famous GM spectrum of internal waves (Garrett & Munk 1972; Cairns & Williams 1976; Garrett & Munk 1979), see (2.3) in the body of the paper. Thus, slightly adjusting the GM spectrum so that its scale-invariant limit matches the power-law behaviour of the convergent stationary solution, we compute the energy flux via the collision integral of the wave kinetic equation. This collision integral contains complete information concerning resonant spectral energy transfers. The computation of the flux is performed numerically. Our expression for these energy fluxes compares favourably with the finescale parametrization formula put forward in Polzin *et al.* (1995).

To characterize the energy fluxes towards high wavenumbers, we investigate the formation of the stationary-wave spectra in the kinetic equation. We therefore analyse and classify the contributions of the various resonant triads that contribute to the kinetic equation. The importance of triads with extreme scale separation were previously identified in the literature (McComas & Bretherton 1977) and named induced diffusion (ID), parametric subharmonic instability (PSI) and elastic scattering (ES). In addition, we point out an additional class of important interactions that are collinear, or almost so, in the horizontal plane, which appear to contribute significantly to the formation of the stationary state and the fluxes of energy.

The paper is written as follows. In § 2, we give the reader the relevant background along with a necessarily brief literature review. In § 3, we analyse the convergence conditions of the collision integral at the infrared and the ultraviolet limits. We perform a rigorous numerical integration paying special attention to accurately integrate integrable singularities of the kinetic equation kernel. We also analyse in detail the nature of the interacting triads contributing to the stationary scale-invariant solution of the kinetic equation. An analytical and numerical analysis of these various contributions is presented

in § 4, highlighting the main physical mechanisms at play. In § 5, we compute the energy fluxes toward the small scales and thereby quantify the total dissipated energy. Finally, we summarize our results in § 6.

2. Background material

2.1. *Internal waves and the GM spectrum*

Garrett and Munk have observed that the internal-wave spectrum is separable in frequency-vertical wavenumbers. In other words, it can be accurately represented as a product of a function of frequency and a function of vertical wavenumber. The GM energy spectrum is therefore represented in the two-dimensional domain of vertical wavenumber m with $m \in [m_{min}, m_{max}]$ and frequency σ with $\sigma \in [f, N]$ as

$$e_{\mathrm{GM}}(m, \sigma) = N_0 N b^2 E A(m) B(\sigma), \tag{2.1}$$

$$A(m) = \frac{2}{\pi} \frac{m_\star}{m_\star^2 + m^2}, \quad B(\sigma) = \frac{2f}{\pi} \frac{1}{\sigma \sqrt{\sigma^2 - f^2}}, \quad m_\star = \frac{3\pi}{b} \frac{N}{N_0}, \tag{2.2a,b}$$

normalized in such a way that $\int_{m_{min}}^{m_{max}} A(m)\,\mathrm{d}m \simeq \int_0^\infty A(m)\,\mathrm{d}m = 1$, $\int_f^N B(\sigma)\,\mathrm{d}\sigma \simeq \int_0^\infty B(\sigma)\,\mathrm{d}\sigma = 1$, and the total energy density (per unit mass) is therefore given by $N_0 N b^2 E$, in units of J kg^{-1}. Here N and $N_0 = 0.00524$ s^{-1} are, respectively, the buoyancy frequency and the reference buoyancy frequency, $f = 2 \times 7.3 \times 10^{-5} \sin(l)$ s^{-1} is the Coriolis parameter computed at latitude $l = 32.5°$, $b = 1300$ m is the scale height of the ocean, $E = 6.3 \times 10^{-5}$ is the GM specification of the non-dimensional energy level and $m_\star$ is a reference vertical wavenumber. Furthermore, $m_{min} = 2\pi(2600 \text{ m})^{-1}$, $m_{max} = 2\pi(10 \text{ m})^{-1}$ are the physical cutoffs imposed by the ocean depth and by wave breaking, respectively.

2.2. *Wave-turbulence interpretation of the GM spectrum*

Despite the GM far reaching combination of simplicity and descriptive power of available field measurements, its phenomenological nature does not necessarily provide an explanation to the underlying physics. Since the 1970s, the concept of nonlinear interactions has become the *leitmotiv* in the search for a physical interpretation of the GM spectrum starting from the primitive equations of a stratified ocean (Olbers 1973, 1976; McComas & Bretherton 1977; Pelinovsky & Raevsky 1977; Voronovich 1979; McComas & Müller 1981; Holloway *et al.* 1986; Müller *et al.* 1986; Caillol & Zeitlin 2000; Lvov & Tabak 2001). The quadratic nonlinearity in the primitive fluid equations and a dispersion relation allowing for three-wave interactions imply that internal waves interact through triads. In a weakly nonlinear regime, three-wave resonant interactions are responsible for slow, net energy transfers between different wavenumbers (Davis *et al.* 2020). This process can be described by a wave kinetic equation, the evolution equation of the action spectrum of the internal wave field (Hasselmann 1966; Zakharov, L'vov & Falkovich 1992; Nazarenko 2011). In the present paper, we use the three-dimensional wavenumber domain $\boldsymbol{p} = (\boldsymbol{k}, m)$, where $\boldsymbol{k}$ and m are the horizontal and the vertical wavenumbers, respectively. Note that $\boldsymbol{k}$ is a two-dimensional horizontal wave vector and we define its norm as $k := |\boldsymbol{k}|$. The dispersion relation of internal gravity waves is given by $\sigma_{\boldsymbol{p}}^2 = f^2 + N^2(k^2/m^2)$, which can be used to switch from one domain to the other, since only two of the three variables k, m and σ are independent. The action spectrum $n(\boldsymbol{k}, m)$ is related to the energy spectrum

$e(\mathbf{k}, m)$ (now both intended as three-dimensional spectra) via $e(\mathbf{k}, m) = \sigma n(\mathbf{k}, m)$, where for simplicity we use the quantities in brackets to specify the domain of dependence of the quantity of interest. We assume horizontal and vertical isotropy, so that we have $e(m, \sigma) = 4\pi k e(\mathbf{k}, m)(\mathrm{d}\sigma/\mathrm{d}k)^{-1}$, after integrating over the horizontal azimuthal angle and considering a positive definite m. Considering the scale-invariant (or non-rotating) limit $f \ll \sigma \ll N$, which yields the scale-invariant dispersion relation (here defined as the positive branch) $\sigma = Nk/|m|$, (2.1) transforms into

$$n_{\mathrm{GM}}(\mathbf{k}, m) = \frac{1}{\pi^3} \frac{Eb^2 N_0 f m_\star}{N} k^{-4}, \tag{2.3}$$

which represents the non-rotating limit of the GM three-dimensional action spectrum, in the horizontal wavenumber–vertical wavenumber domain.

The wave-turbulence theory for internal waves was revisited with the generalized random phase and amplitude formalism (Choi, Lvov & Nazarenko 2004, 2005; Nazarenko 2011) in the series of works (Lvov & Tabak 2001; Lvov, Polzin & Tabak 2004; Lvov *et al.* 2010), where the internal-wave kinetic equation was derived starting from the primitive equations of motion in hydrostatic balance by using isopycnal coordinates. A detailed review is found in the introductory paragraphs of Lvov *et al.* (2010) and will not be repeated here. The main steps can be schematized as follows: (i) the primitive equations of a vertically stratified ocean in hydrostatic balance and with no background rotation are rewritten in isopycnal coordinates under the Boussinesq approximation. The scale-invariant limit of the dispersion relation in the new variables reads (with no background rotation)

$$\sigma(\mathbf{k}, m) = \frac{g}{\rho_0 N} \frac{k}{|m|}, \tag{2.4}$$

where g is the acceleration of gravity, ρ_0 is the reference density and the vertical wavenumber m is now an inverse density. (ii) In the isopycnal formulation, the equations of motion are reduced to Hamiltonian form for the two conjugate fields ϕ and Π, the velocity potential and the normalized differential layer thickness. (iii) The machinery of wave turbulence is applied by switching to Fourier space and introducing the complex canonical normal variables c_p and c^*_{-p}, representing complex amplitudes of the normal modes of the system. Under the assumption of spatial homogeneity, the action spectral density is defined as

$$\langle c_{p_1} c^*_{p_2} \rangle = n_{p_1} \delta_{p_1 - p_2}, \tag{2.5}$$

where $\delta(\cdot)$ is a Dirac delta, and the angular brackets denote averaging on a suitably defined statistical ensemble: under the standard assumptions of random phases and amplitudes (Zakharov *et al.* 1992; Nazarenko 2011), in the joint limit of large box and small nonlinearity the following wave kinetic equation is derived, assuming isotropy in the horizontal plane (for simplicity, here written in the non-rotating limit):

$$\frac{\partial n_p}{\partial t} = \frac{8\pi}{k} \int \left(f^p_{12} |V^p_{12}|^2 \delta_{m-m_1-m_2} \delta_{\sigma_p - \sigma_1 - \sigma_2} \frac{kk_1 k_2}{\Delta_{p12}} - (0 \leftrightarrow 1) - (0 \leftrightarrow 2) \right)$$
$$\times \mathrm{d}k_1 \, \mathrm{d}k_2 \, \mathrm{d}m_1 \, \mathrm{d}m_2, \tag{2.6}$$

where $n_p = n(\mathbf{k}, m; t)$ is the three-dimensional action spectrum defined in (2.5), $f^p_{12} = n_1 n_2 - n_p(n_1 + n_2)$, V^p_{12} is the matrix element describing the magnitude of nonlinear interactions between the triad of wavenumbers p, p_1 and p_2, given below by (3.3).

Furthermore, the two delta functions impose the conservation of vertical momentum and energy in each three-wave interaction. The Δ_{p12}, given by (3.2), is a factor coming from integration of the horizontal momentum delta function, proportional to the area of the triangle with sides k, k_1 and k_2. (iv) The wave kinetic equation (2.6) with dispersion relation (2.4) is fully scale-invariant and the consequent theory of power-law spectra (Zakharov *et al.* 1992) was worked out in Lvov *et al.* (2010). Assuming a solution of type

$$n_p \propto k^{-a}|m|^{-b}, \tag{2.7}$$

the stationary solution corresponding to constant energy flux, i.e. the Kolmogorov–Zakharov (KZ) spectrum, can be derived by Zakharov–Kuznetsov conformal mapping (Zakharov *et al.* 1992) yielding $a = 7/2$, $b = 1/2$:

$$n^{PR}(k, m) = k^{-(7/2)}m^{-(1/2)}. \tag{2.8}$$

Such a solution was derived in Pelinovsky & Raevsky (1977) and again in Lvov & Tabak (2001) and is known as the Pelinovski–Raevski (PR) spectrum. (v) A KZ spectrum is a valid solution of the wave kinetic equation if and only if the locality conditions are satisfied, i.e. when the collision integral on the right-hand side of the wave kinetic equation converges. It turns out that this is not the case for the PR spectrum; more precisely, in the $a - b$ power-law space Lvov *et al.* (2010) found that the collision integral converges only on the segment $b = 0, 3.5 < a < 4$. (vi) On this convergence segment, it was shown by direct numerical integration that the collision integral is zero for $a \simeq 3.7$, locating the scale-invariant stationary solution of the wave kinetic equation at the point $a = 3.7, b = 0$. Since this is not far from the $a = 4, b = 0$ point of (2.3), such a solution has therefore been put forward as the possible theoretical explanation of the GM spectrum provided by wave turbulence.

In the present work. we use the wave-turbulence kinetic equation to analyse how the stationary scale-invariant internal-wave spectrum is formed, and we calculate the corresponding energy fluxes related to this spectrum. This quantity is modelled phenomenologically, as interpretation of the available data, by what is known as the finescale parametrization of the oceanic turbulent mixing (Polzin *et al.* 1995, 2014; Whalen, Talley & MacKinnon 2012; MacKinnon *et al.* 2017; Liang *et al.* 2018), and represents a fundamental building block of the GCM.

3. The convergent stationary solution of the wave kinetic equation

Our starting point is the scale-invariant wave kinetic equation (2.6). In Lvov *et al.* (2010), the locality conditions on the exponents a, b of (2.7) were computed, yielding convergence conditions $b = 0, 3.5 < a < 4$. We repeated those calculations, confirming that for $b \neq 0$ the collision integral is divergent, i.e. corresponds to interactions that are non-local in Fourier space, because of divergence in the infrared or the ultraviolet limits, or both. In the present paper, we focus our attention to the case $b = 0$. We recompute the leading order of the integrand at the boundaries of the kinematic box, showing that the infrared convergence condition gives $a < 4$ and the ultraviolet convergence condition gives $a > 3$. The combination of the two conditions yields a convergence segment $3 < a < 4$, different from the condition $3.5 < a < 4$ found in Lvov *et al.* (2010). The correction to the previous result is due to a second exact cancellation in the ultraviolet divergence, previously undetected. We use a rigorous numerical procedure, with details in the supplementary materials available at https://doi.org/10.1017/jfm.2021.99 (Dematteis & Lvov 2020), to compute the integrable singularities accurately by exploiting the analytical knowledge of

the leading-order terms. By direct numerical computation, we numerically confirm that on the convergence segment the collision integral tends to $-\infty$ as $a \to 3^+$, due to the ultraviolet divergence, and it tends to $+\infty$ as $a \to 4^-$, due to the infrared divergence. Moreover, it is monotonically increasing with a, crossing zero at $a = 3.69$. Numerical convergence is checked to a high degree of accuracy. The independent computation of the convergent stationary spectrum $a = 3.69, b = 0$ is the first important result of the paper, confirming the previous result in Lvov *et al.* (2010), although a correction to the convergence segment has been made.

3.1. *Locality conditions*

Let us consider the wave kinetic equation of internal gravity waves in a non-rotating frame, in hydrostatic balance, and in the scale-invariant limit. This is described by (2.6), with the dispersion relation (2.4), expressed in isopycnal coordinates. By integrating analytically the two remaining Dirac deltas, we simplify the collision integral, reducing it to a double integral. The wave kinetic equation thus takes the following form:

$$
\left.
\begin{aligned}
\partial_t n_{\boldsymbol{p}} &= \mathcal{I}(k, m; a, b) := \int_0^{\infty} \mathrm{d}k_1 \, \mathrm{d}k_2 \, \mathcal{J}(k, k_1, k_2, m), \\
\mathcal{J}(k, k_1, k_2, m) &= \frac{8\pi}{k}(R_{12}^{\boldsymbol{p}} f_{12}^{\boldsymbol{p}} - R_{\boldsymbol{p}2}^{1} f_{\boldsymbol{p}2}^{1} - R_{\boldsymbol{p}1}^{2} f_{\boldsymbol{p}1}^{2}), \\
R_{12}^{\boldsymbol{p}} &= kk_1k_2|V_{12}^{\boldsymbol{p}}|^2 / (|g_{12}^{\boldsymbol{p}\,\prime}| \Delta_{\boldsymbol{p}12}).
\end{aligned}
\right\}
\tag{3.1}
$$

Here $f_{12}^{\boldsymbol{p}} = n_1 n_2 - n_{\boldsymbol{p}}(n_1 + n_2)$ and the area of the triangle of sides k, k_1, k_2, coming from integration over angles under the assumption of isotropy, is given by

$$
\Delta_{\boldsymbol{p}12} = \tfrac{1}{2}\sqrt{2(k^2k_1^2 + k^2k_2^2 + k_1^2k_2^2) - k^4 - k_1^4 - k_2^4}.
\tag{3.2}
$$

The expression of the matrix elements reads (Lvov *et al.* 2010)

$$
\begin{aligned}
V_{\boldsymbol{p}_1\boldsymbol{p}_2}^{\boldsymbol{p}} = \sqrt{kk_1k_2} &\left(\frac{k^2 + k_1^2 - k_2^2}{2kk_1}\sqrt{\left|\frac{m_2^{\star}}{mm_1^{\star}}\right|} + \frac{k^2 + k_2^2 - k_1^2}{2kk_2}\sqrt{\left|\frac{m_1^{\star}}{mm_2^{\star}}\right|} \right. \\
&\left. + \frac{k^2 - k_1^2 - k_2^2}{2k_1k_2}\sqrt{\left|\frac{m}{m_1^{\star}m_2^{\star}}\right|} \right),
\end{aligned}
\tag{3.3}
$$

$$
g_{12}^{\boldsymbol{p}\,\prime} = \frac{\mathrm{sign}(m_1^{\star})k_1}{(m_1^{\star})^2} - \frac{\mathrm{sign}(m_2^{\star})k_2}{(m_2^{\star})^2},
\tag{3.4}
$$

where $m_1^{\star}, m_2^{\star}$ are given by the solution of the resonance conditions, i.e. the joint conservation of momentum and energy in each triadic interaction. Thus, in the four-dimensional space spanned by k_1, k_2, m_1, m_2, the problem is now restricted to the resonant manifold, parametrized by two independent variables k_1 and k_2 as summarized in table 1.

Note the symmetries of the resonant manifold: the solution (Ia) is obtained from solution (Ib) through permutation of the indices $1 \leftrightarrow 2$. We also notice that solutions (IIa), (IIb) reduce to solutions (IIIa), (IIIb), respectively, under permutation of the indices $1 \leftrightarrow 2$.

915 A129-6

Label	Resonance condition	Solutions
(Ia), (Ib)	$\begin{cases} \boldsymbol{p} = \boldsymbol{p}_1 + \boldsymbol{p}_2 \\ \dfrac{k}{\lvert m \rvert} = \dfrac{k_1}{\lvert m_1 \rvert} + \dfrac{k_2}{\lvert m - m_1 \rvert} \end{cases}$	$\begin{cases} m_1^\star = \dfrac{m}{2k}[k \pm k_1 \pm k_2 \pm \sqrt{(k \pm k_1 \pm k_2)^2 \mp 4kk_1}] \\ m_2^\star = m - m_1^\star \end{cases}$
(IIa), (IIb)	$\begin{cases} \boldsymbol{p}_1 = \boldsymbol{p} + \boldsymbol{p}_2 \\ \dfrac{k_1}{\lvert m_1 \rvert} = \dfrac{k}{\lvert m \rvert} + \dfrac{k_2}{\lvert m_1 - m \rvert} \end{cases}$	$\begin{cases} m_2^\star = -\dfrac{m}{2k}[k \mp k_1 - k_2 + \sqrt{(k \mp k_1 - k_2)^2 + 4kk_2}] \\ m_1^\star = m + m_2^\star \end{cases}$
(IIIa), (IIIb)	$\begin{cases} \boldsymbol{p}_2 = \boldsymbol{p} + \boldsymbol{p}_1 \\ \dfrac{k_2}{\lvert m_2 \rvert} = \dfrac{k}{\lvert m \rvert} + \dfrac{k_1}{\lvert m_2 - m \rvert} \end{cases}$	$\begin{cases} m_1^\star = -\dfrac{m}{2k}[k - k_1 \mp k_2 + \sqrt{(k - k_1 \mp k_2)^2 + 4kk_1}] \\ m_2^\star = m + m_1^\star \end{cases}$

Table 1. The six independent solutions to the resonance conditions (Lvov *et al.* 2010).

Based on the condition $b = 0$ in (2.7), we consider a scale invariant solution which is horizontally isotropic and independent of the vertical wavenumber:

$$n_{\boldsymbol{p}} = n(\boldsymbol{p}) \propto k^{-a}. \tag{3.5}$$

Since the collision integral is scale invariant in k, it is sufficient to calculate it for a fixed value (e.g. $k = 1$ for simplicity), and then retrieve the solution for any value of k by using the scale-invariance relation involving the homogeneity degree of the collision integral.

Integration is performed in the kinematic box, defined by the three triangular relations: $k + k_1 \geq k_2$, $k_1 + k_2 \geq k$, $k + k_2 \geq k_1$. We differentiate three different regions of the kinematic box: near-collinear region (A_C and B_C), extreme scale-separated region (the infrared region IR and the ultraviolet region UV), and the region of unclassified triads, denoted as (A_U and B_U), as shown in figure 1. Here, A_C and B_C are named near-collinear regions since the resonant triads tend to the collinear limit approaching their boundary given by $k_2 = \lvert k_1 - k \rvert$, a relationship that can be fulfilled only by degenerate triangles with their sides lying on the same line. The thickness of the regions A_C and B_C is given by the parameter k_{IR}: small values of k_{IR} imply that the resonant triads inside these regions are close to the collinear limit. We refer to IR and UV as the extreme scale-separated regions: for the triads in IR, two wavenumbers have finite horizontal momentum, and one wavenumber has vanishing horizontal momentum. For the triads in UV, two wavenumbers have very large horizontal momentum, and one wavenumber has a much smaller horizontal momentum. All the possible resonances in IR and UV constitute the so-called named triads. Finally, A_U and B_U include all the non-collinear, unclassified triads. Exploiting symmetries, the right-hand side of (2.6), which we denote by $\mathcal{I}(k, m; a, b)$ after introducing the ansatz (2.7), can be reorganized as follows:

$$\mathcal{I}(k, m; a, b) = \left[\left(\int_{A_C} + \int_{A_U} + 2 \left(\int_{B_C} + \int_{B_U} + \int_{IR} + \int_{UV} \right) \right) \right] \mathcal{J}(k, k_1, k_2, m) \, \mathrm{d}k_1 \, \mathrm{d}k_2, \tag{3.6}$$

where a sum over the six solutions to the above resonance conditions is implicit. With $b = 0$, the conditions on the exponent a for convergence of the collision integral on the right-hand side of (3.1) come from the infrared (IR, red in figure 1) and the ultraviolet (UV, dark blue in figure 1) regions of integration. The details for the computation of the following results are given in the supplementary materials (Dematteis & Lvov 2020). Both singularities involve a first and a second cancellation between equal and oppositely signed
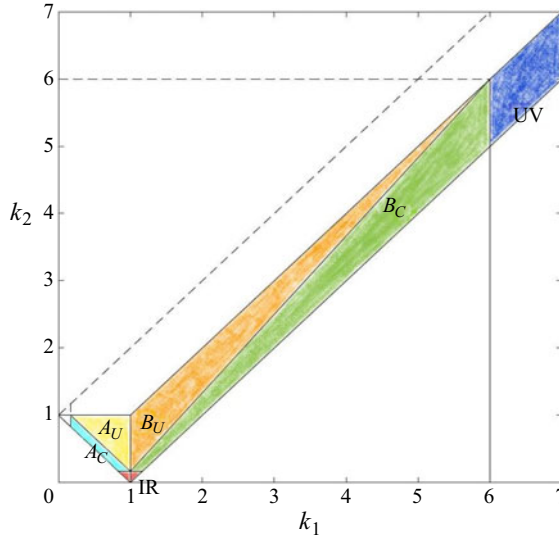
Figure 1. The kinematic box is split into subregions: A_C (light blue), A_U (yellow), B_C (green), B_U (orange), IR (red), UV (blue). Here, A_C and B_C are the near-collinear regions, IR and UV are the extreme scale-separated regions, and A_U and B_U are the unclassified regions. A suitable Zakharov–Kraichnan transformation, see (4.1a,b), maps the regions B_C and B_U into A_C and A_U, respectively.

leading terms. For the infrared contribution, we obtain

$$\mathcal{I}_{\mathrm{IR}} \simeq -16\pi a k^{-2a+4} m \int_0^{k_{\mathrm{IR}}/k} \mathrm{d}x \int_{-x}^x \mathrm{d}y \, x^{-a-1} \frac{y^2(y^2 - x^2)}{\sqrt{x^2 - y^2}} = 2\pi^2 \frac{a}{4-a} mk^{-a} k_{\mathrm{IR}}^{-a+4},$$

(3.7)

where k_{IR} is the (small) height of the red region in figure 1. The integral converges if $a < 4$. Also notice that the integral is positive. For the ultraviolet contribution, we obtain

$$\mathcal{I}_{\mathrm{UV}} \simeq -32\pi a k^{-2a+4} m \int_0^{k/k_{\mathrm{UV}}} \mathrm{d}x \int_0^x \mathrm{d}y \, \frac{k^2}{x^3} x^{a-8} \left[(x-y)^4 + x^2(x-y)^2 \right] / \sqrt{(2x-y)y}$$

$$\simeq -14\pi^2 \frac{a}{a-3} k^{-a+1} mk_{\mathrm{UV}}^{3-a},$$

(3.8)

where k_{UV} is the k_1 coordinate of the left boundary of the ultraviolet region. The integral converges when $a > 3$. Note that this contribution is negative, providing possibility for this contribution to balance the positive contribution from (3.7). This observation will later be exploited in § 4.2 to find the steady-state solution composed of a balance of infrared and ultraviolet contributions. The contribution (3.7) is given by the resonance conditions (Ia) and (IIa), the infrared ID resonances, while the contribution (3.7) is given by the resonance conditions (IIb) and (IIIc), the ultraviolet ID resonances. Both ES and PSI resonances turn out to be subleading.

3.2. Numerical solution: $a = 3.69$

Straightforward numerical integration can be performed only in A_U and B_U, since close to the boundaries the integrand contains integrable singularities. For this reason, numerical integration is performed adopting the following technique for integrable singularities

915 A129-8

(Heath [2002]). We take the leading-order singularity of the integrand, integrate it analytically and add the numerical integral of the difference between the integrand and the leading-order singularity. This way, the integrable singularities are integrated analytically rather than numerically, ensuring accurate results. Notice that a singular behaviour is found not only in the infrared and ultraviolet regions, but also in the collinear regions, due to the vanishing denominator Δ_{p12}. The vanishing of denominator occurs because the area of a triangle with collinear sides tends to zero. The detail of the procedure for each of the five regions is found in the supplementary materials (Dematteis & Lvov [2020]).

To convince the reader that the numerical integration is performed accurately, we show that the discretized integral is independent of the step size of the discretization grid for sufficiently fine grid. This is demonstrated in the supplementary materials (Dematteis & Lvov [2020]).The width of the regions around $k_2 = 0$ is determined by the parameter k_{IR}, while the cut at large k's is performed at $k_1 = k_{UV}$. For the result to be general, it must be independent of the choice of k_{IR} and k_{UV}, as long as they are finite numbers, k_{IR} being sufficiently small and k_{UV} sufficiently large. It turns out this is indeed the case in our numerics. In the supplementary materials (Dematteis & Lvov [2020]), we show how convergence is reached as k_{UV} increases, as the neglected contribution in UV vanishes. Independence of the result upon variations of k_{IR} is even more robust.

According to our results, the stationary spectrum of internal waves is given by

$$n(k, m) \propto k^{-a_0}, \quad a_0 \simeq 3.69. \tag{3.9}$$

The result in figure 2, obtained with a choice $k_{UV} = 1/k_{IR} = 16$, confirms convergence of the collision integral for $3 < a < 4$: divergence of the integral is found both as $a \to 3^+$ and $a \to 4^-$. In figure 2, we show the contributions of each region of the kinematic box. The $a = 3$ divergence is negative and due to the region UV (ultraviolet). The contribution of UV is always negative and tends to zero as $a \to 4$. On the other hand, the $a = 4$ divergence is positive and due to the region IR. The contribution of IR is always positive and tends to zero as $a \to 3$. At the stationary solution $a = a_0$, the contributions of IR, A_U, B_U, UV are close to zero, while the contributions of A_C (positive) and B_C (negative) are large and cancel out. Notice that the results are obtained for A_C and B_C being thin slices of width $1/16$: the points in the collinear region correspond to triads of wave vectors that have angles between each other's horizontal components of $3°$ or less!

Let us consider an arbitrary reference number $k = 1$. The sign of the integrand in figure 2(*b*) indicates the direction of the energy transfers. We see from figure 2 that the contribution from the wavenumbers with $k_1 < 1$ is positive. Therefore, there is a net energy flow from wavenumbers smaller than reference number $k = 1$ to the reference wavenumber $k = 1$. On the other hand, the contribution from the wavenumbers with $k_1 > 1$ is negative. Consequently the wavenumber $k = 1$ constantly pumps energy towards higher wavenumbers. Therefore, we conclude that the energy transfer is directed towards high horizontal wavenumbers. We elaborate on this further in § 5.

The outflowing energy from the small-wavenumber near-collinear triads is balanced by the inflowing energy at the large-wavenumber near-collinear triads, implying a stationary flow mediated by $k = 1$, which is represented as a thick arrow in figure 2. The outflowing energy from the infrared region is balanced by the inflowing energy entering the ultraviolet region, giving a stationary energy flow between these two regions mediated by $k = 1$. This energy transfer is represented as a thin directed arrow connecting the two regions. The quantitative justification of the balance is given by figure 2(*a*).

The value of the exponent appears to be characterized importantly by a balance of the regions A_C and B_C. This suggests that a suitable transformation mapping one region into
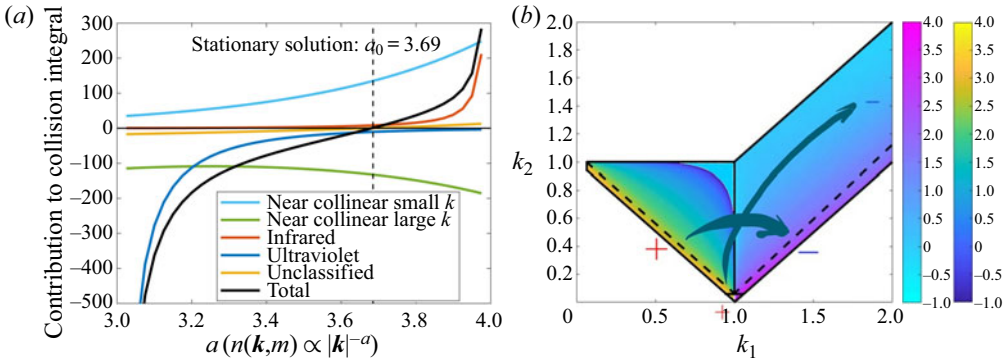
Figure 2. (*a*) Contributions of each subregion (as split in (3.6)) to the integral for $b = 0$ and varying a. (*b*) The base-10 logarithm of the magnitude of the integrand is shown, for the solution $a = 3.69$, $b = 0$. The colourmap labelled by the left colourbar indicates negative values, and the right colourbar indicates positive values. Also, we show here the schematic representation of the downscale energy transfers. The thicker arrow represents the stationary transfer between near-collinear regions, and the thinner arrow between regions with extreme scale separation. The fluxes of energy are explained in § 5.

the other could potentially make the search for the steady self-similar spectrum amenable to analytical treatment. This task is addressed in the next section.

4. Analysis of the contributions to the stationary solution

We consider the reorganized expression of the collision integral in (3.1). Let us introduce the following Zakharov–Kraichnan transformations:

$$\left\{ k_1 = \frac{k^2}{\tilde{k}_1} \quad k_2 = \frac{k\tilde{k}_2}{\tilde{k}_1} \right\}, \quad \left\{ k_2 = \frac{k^2}{\tilde{k}_2} \quad k_1 = \frac{k\tilde{k}_1}{\tilde{k}_2} \right\}, \quad (4.1a,b)$$

and notice that under the first transformation the regions B_C and B_U are mapped into A_C and A_U, respectively, if the choice $k_{\mathrm{UV}} = k^2/k_{\mathrm{IR}}$ is made. In the following, we consider the contributions from the three types of regions (near-collinear, extreme scale-separated and unclassified) separately, with the goal of locating the regions and the resonances that matter the most and the ones that are negligible.

4.1. *Collinear limit*

We start by analysing the contributions in the regions A_C and B_C by decomposing them into separate subcontributions from the three resonance types (I), (II) and (III) (see table 1). The different contributions are plotted in figure 3. We realize that in the region A_C the leading contribution is given by the resonance condition (I), while in region B_C the leading contribution is given by the resonance condition (II). Let us consider only these two contributions, naming them the main collinear contributions:

$$\mathcal{I}_{A_C} + 2\mathcal{I}_{B_C} \simeq \int_{k_{\mathrm{IR}}}^{1-k_{\mathrm{IR}}} \mathrm{d}k_2 \int_0^{k_{\mathrm{IR}}} \mathrm{d}x \frac{T_{k_1,k-k_1}^k}{\sqrt{2kk_1(k-k_1)x}}$$
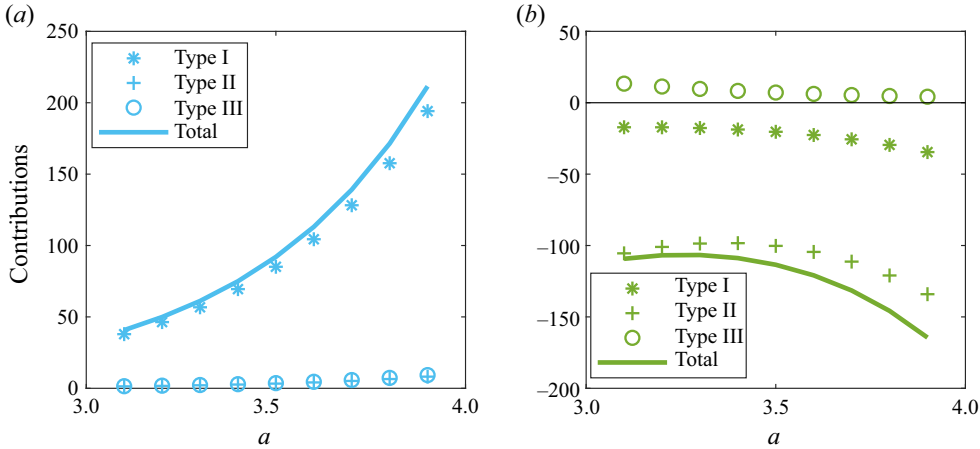
Figure 3. The contributions from A_C (*a*), and B_C (*b*) (the latter multiplied by 2 to account for its symmetric B'_C by permutation $k_1 \leftrightarrow k_2$) are split into their subcontributions from the three resonance types, showing that A_C is dominated by the contribution (I), while B_C is dominated by the contribution (II). Computing the balance between these two contributions leads to a theoretical estimate $a = 7/2$.

$$-\int_{1+k_{IR}}^{k_{UV}} dk_2 \int_0^{k_{IR}} dx \, \frac{T^{k_1}_{k,k_1-k}}{\sqrt{2kk_1(k_1-k)x}}$$

$$-\int_{1+k_{IR}}^{k_{UV}} dk_2 \int_0^{k_{IR}} dx \, \frac{T^{k_2}_{k,k_2-k}}{\sqrt{2kk_2(k_2-k)x}}, \tag{4.2}$$

where $T^0_{12} = kk_1k_2|V^0_{12}|^2 f^0_{12}/|g^0_{12}{}'|$. Transforming the integral into an integral in the region A_C, by using the symmetries of (4.1*a,b*) (with $k_{UV} = k^2/k_{IR}$) and the scale-invariant properties of the integrand, we obtain (renaming $\tilde{k}_1 \to k_1$, $\tilde{k}_2 \to k_2$)

$$\mathcal{I}_{A_C} + 2\mathcal{I}_{B_C} \simeq \int_0^{k_{IR}} dx \int_{k_{IR}}^{1-k_{IR}} dk_2 \, \frac{T^k_{k_1,k-k_1}}{\sqrt{2kk_1(k-k_1)x}} \left[1 - \left(\frac{k}{k_1}\right)^{r+3} - \left(\frac{k}{k_2}\right)^{r+3}\right], \tag{4.3}$$

where r is the degree of homogeneity of the integrand: $r = 3 - 2a$ (same dependence on k as in the computation of the PR spectrum). We used the property of the Zakharov–Kraichnan transformation for an homogeneous function of degree r with respect to horizontal wave numbers:

$$\mathcal{J}(k_1, k, k_2, m) = \mathcal{J}\left(\frac{k}{\tilde{k}_1}k, \frac{k}{\tilde{k}_1}\tilde{k}_1, \frac{k}{\tilde{k}_1}\tilde{k}_2, m\right) = \left(\frac{k}{\tilde{k}_1}\right)^r \mathcal{J}(\tilde{k}, \tilde{k}_1, \tilde{k}_2, m), \tag{4.4}$$

and a factor $(k/\tilde{k}_1)^3$ appeared due to the Jacobian of the coordinate change. Now, we notice that if $r + 3 = -1$, the integrand contains a factor $[k - k_1 - k_2]$. Since we are considering the near-collinear region, horizontal momentum conservation implies that such a factor vanishes (more precisely, it would vanish in the limit $k_{IR} \to 0$): A_C is a thin slice lying on the line $k_2 = k - k_1$. Therefore, we have that $\mathcal{I}_{A_C} + 2\mathcal{I}_{B_C} = 0$ for $6 - 2a = -1$, which determines the value of $a = 7/2$ as the critical exponent. We have therefore found analytically the steady-state solution for the reduced kinetic equation dominated by the balance between the contribution of type (I) in the region A_C and the
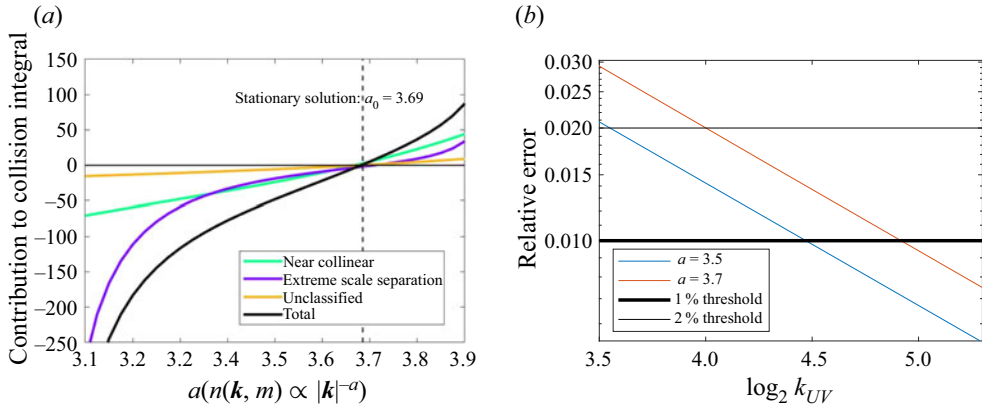
Figure 4. (*a*) The net contribution of the three types of triads, showing that each type balances to zero independently at the convergent stationary solution. (*b*) Relative error of (3.8) with respect to the fully numerically integrated contribution of region UV. Around $a = 3.7$, we see that a choice of $k_{UV} = 16$ ($y = 4$) implies an error of approximately 2 %, which we consider acceptable. Thus, we consider $k_{UV} = 16$ as a reasonable delimitation of the ultraviolet region, as well as $k_{IR} = 1/16$ as the delimitation of the infrared region.

contribution of type (II) in the region B_C, which are the largest contributions from the near-collinear regions. This solution is therefore given by

$$n(k, m) = k^{-(7/2)}m^0. \tag{4.5}$$

Since this solution is close to the PR spectrum (2.8), we propose to call this solution the modified PR spectrum. The difference between (4.5) and (2.8) is that the latter is the formal solution, corresponding to a non-local spectrum (i.e. implying a divergent collision integral). The former solution, on the other hand, is a physically relevant solution corresponding to a local action spectrum (i.e. whose collision integral is finite). Note, however, that a part of the resonances have been neglected.

The result $a = 7/2$ coming from the collinear limit of (4.3) involves only the two leading contributions in figure 3. This observation provides an intuition on how the exponent a is determined by the kinetic equation. The sum of the subdominant contributions in figure 3 is negative and almost independent of a. When added to the main contribution crossing zero at $a = 7/2$, this negative contribution makes the zero-crossing point shift toward the right and in figure 4(*a*) the total collinear contribution is shown to cross zero at $a \simeq 3.69$.

4.2. *Extreme scale-separated triads*

In this section, we consider the contribution that comes from the extreme scale-separated triads, the sum of the infrared and the ultraviolet contributions. The former is positive and tends to $+\infty$ as $a \to 4^-$; the latter is negative and tends to $-\infty$ as $a \to 3^+$. In figure 4(*a*), we show the total contribution of the extreme scale-separated resonances and we observe numerically that it crosses zero around $a \simeq 3.69$, too. In § 3.1, we proposed a balance between positive infrared (3.7) and negative ultraviolet (3.8) contributions as a way to form the steady-state spectrum of internal waves. This balance hinges upon the choice $k_{UV} = k^2/k_{IR}$, as explained in § 4.1.

In figure 4, we show the relative error of the leading-order analytical expression (3.8), with respect to the numerically computed contribution, as a function of k_{UV}. The result is shown for $a = 3.5$ and $a = 3.7$. Using the expression $k_{UV} = 2^y$, with $k = 1$, we observe that the analytical approximation is good starting from values of

915 A129-12

y between 4 and 5. We choose y (and therefore k_{UV} and k_{IR}) large enough for an accurate approximation with the leading-order expression (3.8) (or (3.7)), yet small enough so that all extreme scale-separated triads (3.8) and (3.7) are actually included in the ultraviolet and infrared regions. We make an arbitrary choice $y = 4$ ($k_{UV} = 1/k_{IR} = 16$) so that the leading-order error of (3.7) and (3.8) is approximately 2 % (see figure 4). Our results are insensitive to this specific choice. The balance between the two expressions gives

$$\left.\begin{array}{l} 2\pi^2 \dfrac{a}{4-a} k_{IR}^{4-a} = 14\pi^2 \dfrac{a}{a-3} \dfrac{1}{k_{IR}^{3-a}} \\[4mm] h_y(a) := (2a-7)y\log 2 = \log 7 + \log\left(\dfrac{4-a}{a-3}\right) =: g(a). \end{array}\right\} \tag{4.6}$$

First, we notice that the presence of a factor 7 on the right-hand side breaks the symmetry that would imply the two contributions balance out at $a = 7/2$, in the middle of the convergence interval $(3, 4)$. Secondly, we notice that the function $g(a)$ has an inflection point at $a = 7/2$, making its Taylor expansion of first order have an error of third order. Using linear interpolation centred at $a = 7/2$, $g_{7/2}(a) = \log 7 - 2(2a - 7)$, as an accurate approximation to $g(a)$, demanding that $h_y(a) = g_{7/2}(a)$, we obtain

$$a = \frac{7}{2} + \frac{\log 7}{2y\log 2 + 4}. \tag{4.7}$$

If we adopt $y = 4$, as chosen throughout the paper, we obtain the solution $a \simeq 3.70$. Using $y = 5$ would yield a solution $a \simeq 3.68$.

In this section, we have shown how the formation of the stationary solution of the wave kinetic equation can be interpreted via two independent balances, between near-collinear triads and between the ID triads of the extreme scale-separated regions. This is consistent with recent results from direct numerical simulations where the dominating interactions were located in the ID regime but also throughout all of the interval $k_1 \in [0, 1.4k]$ (Pan *et al.* 2020). Despite the latter effect was investigated in Pan *et al.* (2020) as a broadening of ID due to large nonlinearity, we find that it may be consistent with the collinear resonances depicted in figure 2(*b*).

5. Downscale energy transfers

5.1. *Physical dimensions and energy conservation*

Using the scale-invariant properties of the collision integral, the right-hand side of (3.1) can be rewritten considering the appropriate physical dimensions as

$$I(\mathbf{k}, m) = |m|^{-2b+1} k^{-2a+4} (V_0 A)^2 \mathcal{I}(k = 1, m = 1; a, b), \tag{5.1}$$

where $\mathcal{I}(k = 1, m = 1; a, b)$ is non-dimensional, V_0 is the dimensional prefactor of the matrix element defined below in (5.5) and A is the prefactor of the GM spectrum defined in (2.2*a*,*b*) above. A simple way to check the dimensional consistency of the prefactor in (5.1) is to consider the contribution from the extreme scale-separated region, (4.6), which is analytically tractable:

$$2\pi^2 \frac{a}{4-a} k^{-a} k_{IR}^{4-a} - 14\pi^2 \frac{a}{a-3} \frac{k^{-a+1}}{k_{IR}^{3-a}}$$

$$= mk^{-2a+4} \left(2\pi^2 \frac{a}{4-a} x_{IR}^{4-a} - 14\pi^2 \frac{a}{a-3} x_{IR}^{a-3}\right), \tag{5.2}$$

where $x_{IR} = k_{IR}/k$ and the term in brackets is a non-dimensional function of the exponent a that vanishes at $a = a_0$. The factor $(V_0 A)^2$ comes from having both the matrix elements and the spectrum to the second power in the collision integral, and by introducing the appropriate dimensional constants that have been omitted so far. The dimensional properties of the collision integral are indeed the same also in the other integration regions.

Next, we compute the spectral energy fluxes, recalling that the energy density is given by

$$e(k, m) = 2\pi k \sigma(k, m) n(k, m), \quad \sigma(k, m) = \alpha \frac{k}{|m|}, \quad \text{with } \alpha = \frac{g}{\rho_0 N}, \quad (5.3a,b)$$

where the scale-invariant dispersion relation (2.4) is used. Using (5.1), the stationary-wave kinetic equation for the energy density assumes the simple form

$$\dot{e}(k, m) = 2\pi (A V_0)^2 k^{-2a+6} m^{-2b} \mathcal{I}(k = 1, m = 1; a, b) = 0. \quad (5.4)$$

5.2. *Dimensional prefactors*

The dimensional factor coming from the matrix elements in (5.1) is given by

$$|V_0|^2 = \frac{N}{32\rho_0}. \quad (5.5)$$

The factor A is the dimensional prefactor of the GM spectrum, our observational input for the oceanic wave field. The procedure to obtain A is explained in the rest of this paragraph. The non-rotating limit of the GM spectrum in $k - m$ coordinates is given by (2.3). However, in isopycnal coordinates the spectrum needs to be multiplied by a factor $N^2 \rho_0/g$, which gives

$$n_{GM}(k, m) = \frac{1}{\pi^3 g} E b^2 N_0 N \rho_0 f m_\star k^{-4}, \quad m_\star = 3\pi \frac{N}{b N_0}, \quad (5.6)$$

where $E = 6.3 \times 10^{-5}$ is the non-dimensional energy level, $b = 1300$ m, $\rho_0 = 1000$ kg m^{-3}, $N_0 = 0.00524$ s^{-1} and $f = 2 \cdot 7.3 \times 10^{-5} \sin(l)$ (at latitude $l = 32.5°$). (A prefactor of 4 instead of 3 is known to imply a more accurate asymptotic fit in the large-wavenumber regime (Polzin & Lvov 2011). However, for simplicity here we keep the factor appearing in the original 1976 GM parametrization as is. We will see that the choice does not affect the order of magnitude of the estimate of the flux.) The values given here are the ones of the standard GM parametrization. Since for the GM spectrum we have $a = 4$ instead of $a = 3.69$, we introduce the modified version of (5.6):

$$n_{GM,c}(k, m) = \frac{1}{\pi^3 g} E b^2 N_0 N \rho_0 f \frac{m_\star}{k_\star^{(1-s)/2}} k^{-(4-(1-s)/2)}, \quad k_\star = m_\star/r, \quad (5.7)$$

where $s = 2a - 7 = 0.38$. This is a slightly less steep, dimensionally consistent version. The non-dimensional parameter $r = N/f$ quantifies the horizontal-to-vertical anisotropy (Polzin & Lvov 2011). Now, the GM spectrum is normalized so that the total energy is expressed in units of J/kg, as usual in physical oceanography. On the other hand, in the wave-turbulence formalism, the total energy is expressed as a density per unit of volume of the physical space. Here, the physical space has units of kg m^{-1}, given by an area in the horizontal directions times a density in the vertical. It is, therefore, possible to switch from one representation to the other multiplying by the appropriate density, which in this case is the characteristic density of the isopycnal coordinates, $\Pi = g/N^2$, in units of metres

(normalized differential thickness of an isopycnal layer). So, we obtain the equivalence: $n_{WKE} = n_{GM} \cdot g/N^2$, which applied to (5.7) finally gives the dimensionally consistent factor

$$A = \frac{1}{\pi^3} Eb^2 \rho_0 f \frac{N_0}{N} \frac{m_\star}{k_\star^{(1-s)/2}}. \tag{5.8}$$

5.3. *Dissipated power at high wavenumbers*

In order to compute the energy flux towards high wavenumbers, we need to consider the physical cutoffs of the problem. Natural cutoffs are imposed on the vertical wavenumber by the depth of the ocean and by the wave breaking cutoff, and on the frequency by the inertial frequency and the buoyancy frequency,

$$m_{min} = \frac{2\pi g}{\rho_0 N^2} \times (2600 \text{ m})^{-1}, \quad m_{max} = \frac{2\pi g}{\rho_0 N^2} \times (10 \text{ m})^{-1}, \quad \sigma_{min} = f, \quad \sigma_{max} = N. \tag{5.9a–d}$$

These limiting values define a rectangle in $\sigma - m$ space that translates into a trapezoid in $k - m$ space, with inclined sides given by

$$k_{min}(m) = \frac{f}{\alpha} m, \quad k_{max}(m) = \frac{N}{\alpha} m. \tag{5.10a,b}$$

The collision integral contains all of the necessary information on the spectral energy transfers. In the following, we compute numerically the outflowing power at high wavenumbers from computation of the contribution of the resonant triads with an output wavenumber such that $m > m_{max}$ or $k > k_{max}(m)$, i.e. assuming that the production of a wave beyond the physical high wavenumber cutoff results in complete dissipation of its energy. At the same time, it is assumed that the region within the physical cutoffs is an inertial range with no sources nor sinks, where energy is transferred exclusively via resonant interactions.

Let us define the part of the collision integral which contributes to the dissipation of energy by transferring it beyond the dissipation cutoffs:

$$\left.\begin{array}{l} I_{diss}(\boldsymbol{k}, m; k_{max}) := \dfrac{N^2}{g} (V_0 A)^2 \alpha^{-1} |m|^{-2b+1} k^{-2a+4} \mathcal{I}_{diss}(\kappa), \\[4mm] \mathcal{I}_{diss}(\kappa) = \displaystyle\int_{\Omega_h(\kappa)} \mathcal{J}(k = 1, k_1, k_2, m = 1) \mathrm{d}k_1 \, \mathrm{d}k_2, \end{array}\right\} \tag{5.11}$$

where $\kappa = k_{max}/k$ and $\Omega_h(\kappa)$ is the set of triads transferring energy to output waves beyond the horizontal dissipation cutoff k_{max}, and is defined in table 2. Moreover, a factor N^2/g is added to account for transition to isopycnal coordinates, the inverse of the factor in (5.8). Here, $I_{diss}(\boldsymbol{k}, m; k_{max})$ quantifies the amount of wave action that wavenumber $\boldsymbol{p}$ sends via resonant interactions beyond the dissipation threshold k_{max}, per unit time and per unit volume of Fourier space.

The power (per unit of m) dissipated beyond k_{max} at fixed m (now considered as the positive definite magnitude of m) is related to the integral of $I_{diss}(\boldsymbol{k}, m)$ for all values of k:

$$F_{diss}(m) = \int_{k_{min}}^{k_{max}} 4\pi k \omega(\boldsymbol{p}) I_{diss}(\boldsymbol{k}, m; k_{max}) \, \mathrm{d}k$$

Input	Output	$\Omega_h(\kappa)$	$\Omega_v(\mu)$
		$k_1 > \kappa, k_2 > \kappa$	$|m_1| > \mu, |m_2| > \mu$
		$k_1 > \kappa, k_2 < \kappa :$ weight $\dfrac{\sigma_1}{\sigma_1 + \sigma_2}$	$|m_1| > \mu, |m_2| < \mu :$ weight $\dfrac{\sigma_1}{\sigma_1 + \sigma_2}$
$\boldsymbol{p}$	$\boldsymbol{p}_1, \boldsymbol{p}_2$	$k_1 < \kappa, k_2 > \kappa :$ weight $\dfrac{\sigma_2}{\sigma_1 + \sigma_2}$	$|m_1| < \mu, |m_2| > \mu :$ weight $\dfrac{\sigma_2}{\sigma_1 + \sigma_2}$
$\boldsymbol{p}, \boldsymbol{p}_2$	$\boldsymbol{p}_1$	$k_1 > \kappa, k_2 < \kappa$	$|m_1| > \mu, |m_2| < \mu$
$\boldsymbol{p}, \boldsymbol{p}_1$	$\boldsymbol{p}_2$	$k_1 < \kappa, k_2 > \kappa$	$|m_1| < \mu, |m_2| > \mu$

Table 2. All of the non-negligible contributions for $\kappa > 1$ are negative (see (*b*) of figures 2 and 3). The same holds for $\mu > 1$. Thus, wavenumber $\boldsymbol{p}$ is always an incoming wave in the triads here considered. The table represents the conditions under which every type of resonance results in the dissipation of energy due to at least one output beyond the dissipation cutoffs. During the numerical computation of the integrals C_h and C_v, these conditions are applied for every point of the kinematic box. In the case of a decay into two waves of which only one is dissipated, only the fraction of energy of the dissipated wave must be accounted for, multiplying the contribution by the weight shown in the table.

$$= \frac{N^2}{g} \int_{k_{min}}^{k_{max}} 4\pi |m|^{-2b+1} k^{-2a+5} \alpha \frac{k}{|m|} (V_0 A)^2 \alpha^{-1} \mathcal{I}_{diss}(\kappa) \mathrm{d}k$$

$$= 4\pi \frac{N^2}{g} (V_0 A)^2 k_{max}^{-s} C_h, \quad \text{with } C_h := \int_1^{N/f} \kappa^{s-1} \mathcal{I}_{diss}(\kappa) \mathrm{d}\kappa, \qquad (5.12)$$

where we recall that $s = 2a - 7 = 0.38$, and $b = 0$. In a similar fashion, we can obtain an analogous relation for the energy flux dissipated vertically at vertical wavenumbers larger than m_{max}:

$$\left.\begin{aligned} G_{diss}(k) &= 4\pi \frac{N^2}{g} (V_0 A)^2 k^{-(1+s)} m_{max} C_v, \quad C_v := \int_1^{m_{max}/m_{min}} \mu^{-2} \mathcal{K}_{diss}(\mu) \mathrm{d}\mu, \\ \mathcal{K}_{diss}(\mu) &= \int_{\Omega_v(\kappa)} \mathcal{J}(k=1, k_1, k_2, m=1) \, \mathrm{d}k_1 \, \mathrm{d}k_2, \end{aligned}\right\} \tag{5.13}$$

where $\mathcal{K}_{diss}(\mu)$ ($\mu = m_{max}/m$) is the analogue of $\mathcal{I}_{diss}(\kappa)$ in the vertical direction, i.e. the collision integral restricted to the triads with output waves beyond the m_{max} threshold. The conditions defining Ω_v are found in table 2. These integrals are computed numerically. The computation of C_h is quite straightforward since the kinematic box is expressed in horizontal wavenumber coordinates. The quantity $\mathcal{I}_{diss}(\kappa)$ is computed inside a loop spanning all values of κ, checking the constraint of $\Omega_h(\kappa)$ for every point. Note that since the position of the right boundary depends on m, (5.10*a,b*), in the computation of $\mathcal{I}_{diss}(\kappa)$ we have to impose that $k_1 > k_{max} m_1/m$ (or the same for k_2) for point (k_1, m_1) to be past the absorbing boundary. For the computation of C_v, on the other hand, at every loop iteration we have to integrate over all of the kinematic box to compute $\mathcal{K}_{diss}$ and check point by point whether m_1 or m_2 have 'crossed' the boundary at m_{max} (which is independent of k).

One important point requires particular care. In the previous sections, we relied upon the leading order of the infrared contribution of (3.7), which is obtained after the second cancellation where a negative singularity for $k_1 > 1$ cancels exactly with a positive singularity for $k_1 < 1$. However, since now in (5.11) we consider an integration region where $k_1 > \kappa > 1$, the positive singularity due to $k_1 < 1$ is no longer present and thus the use of (3.7) is not justified. In the integrand of (5.11), whose expression is found in the supplementary materials (Dematteis & Lvov 2020), the finite point singularity therefore
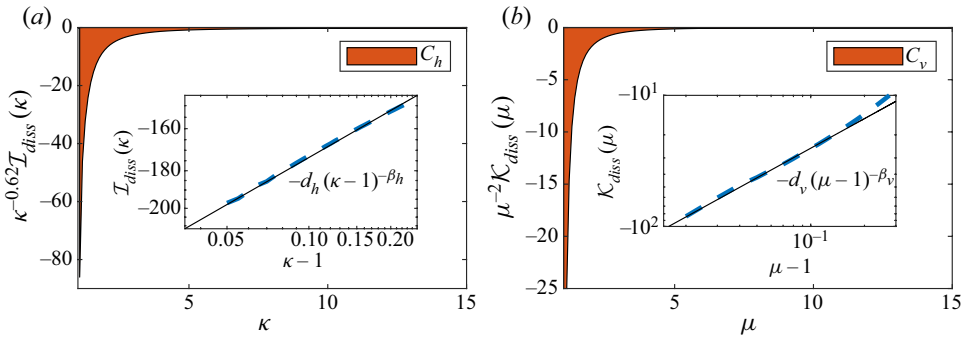
Figure 5. Panels (*a*) and (*b*) show the integrands of C_h and C_v, respectively, and the areas coloured in red represent C_h and C_v themselves. Both integrals have a finite point integrable singularity (the exponents β_h and β_v are in the interval $(0, 1)$) at their left boundaries: the insets show the asymptotic power-law scaling of the singularities.

has exponent $-a + 3/2$ rather than the $-a + 2$ resulting after the second cancellation (leading to (3.7)). Integrating twice according to (5.11), the exponent of the singularity of the integrand defining C_h in (5.12) is $\beta_h = -a + 7/2 \simeq 0.19$. Numerical computation of $\mathcal{I}_{diss}(\kappa)$ as $\kappa \to 1^+$ confirms this analytical prediction and gives a best least square fit of $\mathcal{I}_{diss}(\kappa) \sim -d_h(\kappa - 1)^{-\beta_h}$, for $\kappa - 1 \ll 1$, with $d_h = 127 \times 8\pi$, $\beta_h = 0.19$. An analogous computation for the integral C_v defined in (5.13) leads to a best-fit scaling of its integrand of $\mathcal{K}_{diss}(\mu) \sim -d_v(\mu - 1)^{-\beta_v}$, for $\mu - 1 \ll 1$, with $d_v \simeq 9.0 \times 8\pi$, $\beta_v \simeq 0.75$. In this case, an analytical evidence of the exponent is not simply available since the kinematic box is not expressed in vertical wavenumber coordinates. In figure 5, we show the rapidly decaying behaviour of the integrands of C_h and C_v. Therefore, C_h and C_v are 'universal constants' which are relatively insensitive to the limits of integration in (5.12) and (5.13). The figure also shows a closer look to the scaling of the singularities as $\kappa \to 1^+$ and $\mu \to 1^+$, with the respective best-fit scalings. Therefore we obtain:

$$C_h \simeq \int_1^{N/f} \kappa^{s-1}\mathcal{I}_{diss}(\kappa) \simeq -\frac{d_h k_{\mathrm{IR}}{}^{1-\beta_h}}{1 - \beta_h} + \int_{1+k_{\mathrm{IR}}}^{N/f} \mathrm{d}\kappa \kappa^{s-1}\mathcal{I}_{diss}(\kappa)$$

$$\simeq -8\pi(16.6 + 54.6 + 10.2) \simeq -8\pi \times 81.4. \qquad (5.14)$$

Here, the three numbers 16.6, 54.6 and 10.2 represent the partial contributions by the infrared ID interactions, near-collinear interactions and unclassified interactions, respectively. The ultraviolet contribution is negligible. Then, choosing a value $\mu_{\mathrm{IR}} = 1/16$ to delimit the infrared region for vertical wavenumbers, we have

$$C_v \simeq \int_1^{m_{max}/m_{min}} \mu^{-2}\mathcal{K}_{diss}(\mu) \simeq -\frac{d_v \mu_{\mathrm{IR}}{}^{1-\beta_v}}{1 - \beta_v} + \int_{1+\mu_{\mathrm{IR}}}^{m_{max}/m_{min}} \mathrm{d}\mu \, \mu^{-2}\mathcal{K}_{diss}(\mu)$$

$$\simeq -8\pi(18.0 + 14.0 + 3.1) \simeq -8\pi \times 35.1. \qquad (5.15)$$

Again, the numbers 18.0, 14.0 and 3.1 represents infrared (ID), near-collinear and unclassified contributions, respectively, with a negligible contribution from the ultraviolet regions.

Now, we compute the power crossing the k_{max} boundary, denoted as P_h (horizontal boundary) and the power crossing the m_{max} boundary, denoted as P_v (vertical boundary),

via

$$P_h = \int_{m_{min}}^{m_{max}} F_{diss}(m)\, dm = D_h(1-s)^{-1}\left(\frac{N}{\alpha}\right)^{-s}(m_{max} - m_{min})^{1-s},$$
$$P_v = \int_{(f/\alpha)m_{max}}^{(N/\alpha)m_{max}} G_{diss}(k)\, dk = D_v s^{-1}\left[\left(\frac{f}{\alpha}\right)^{-s} - \left(\frac{N}{\alpha}\right)^{-s}\right]m_{max}^{1-s},$$

(5.16)

where

$$D_h = 4\pi\frac{N^2}{g}(V_0 A)^2 C_h, \quad D_v = 4\pi\frac{N^2}{g}(V_0 A)^2 C_v \qquad (5.17a,b)$$

Using (5.5), (5.8), (5.16) and (5.17a,b), we obtain

$$P_h = \frac{\Gamma C_h}{1-s}\left[1 - \left(\frac{\ell}{2b}\right)^s\right]f^{1+s}N^2 E^2,$$
$$P_v = \frac{\Gamma C_v}{s}\left[1 - \left(\frac{f}{N}\right)^s\right]fN^{1+s}E^2,$$
$$\Gamma = \frac{3}{4\pi^3}\left(\frac{3\ell}{2b}\right)^s\frac{\rho_0 b^2 N_0^{1-s}}{g\ell}, \quad s = 0.38, \quad \ell = 10\ \text{m}.$$

(5.18)

In figure 6, a graphical interpretation of the computations in the above paragraph is shown. The physical cutoffs define a rectangular box (figure 6a) within which energy is transferred through resonant interactions toward high vertical wavenumbers and high horizontal wavenumbers. If energy is provided by large-scale forcing at low frequency, for simplicity represented as a mesoscale eddy in the figure, it ends up being dissipated at high frequencies or high wavenumbers, represented as wave breaking with generation of turbulent vortices. In $k - m$, space this inertial box translates into a trapezoid whose lateral sides are straight lines defined by the dispersion relation. The integrals in (5.16) quantify the contribution to the dissipated power along the dissipative sides of the box. In the figure, the red areas quantify how dissipation is distributed along these dissipative sides of the inertial box.

Equation (5.18) is the main result of our paper. The outgoing power toward large wavenumbers is the quantity that is modelled by the finescale parametrization formula of ocean mixing (Polzin *et al.* 1995) as

$$P_{fs} = (1.9 \times 10^7\ \text{m}^2)\cosh^{-1}\left(\frac{N}{f}\right)fN^2 E^2, \qquad (5.19)$$

which is in agreement with (5.18) regarding the dependence upon the main physical parameters, if the lower-order corrections $(f/N)^s$ and $\cosh^{-1}(N/f)$ are neglected. The predicted intensities can also be compared directly, using the standard parameters of the GM spectrum (5.6) with $N = N_0$, which yields

$$P_h \simeq -0.5 \times 10^{-8}\ \text{W kg}^{-1},$$
$$P_v \simeq -1.5 \times 10^{-8}\ \text{W kg}^{-1}.$$

(5.20)

This amounts to a total dissipated power

$$P_{tot} = P_h + P_v \simeq -2.0 \times 10^{-8}\ \text{W kg}^{-1}, \qquad (5.21)$$

which is negative since it is lost by the wave system considered. With the same parameters and the same sign convention, the finescale parametrization formula predicts a total
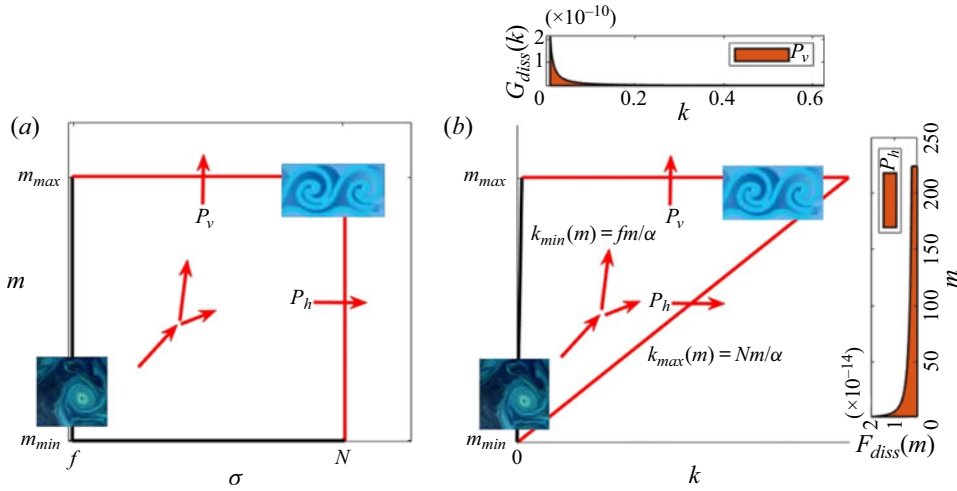
Figure 6. (*a*) The inertial box in $\sigma - m$ space. (*b*) The inertial box in $k - m$ space. The low frequency energy forcing is represented in the picture as a mesoscale eddy, while wave breaking (with generation of turbulent vortices) represents dissipation at high wavenumbers. The distribution of energy dissipation along the absorbing boundaries is depicted in the two insets showing $F_{diss}(m)$ and $G_{diss}(k)$, whose integrals (red area) give, respectively, P_h and P_v, (5.16). In these two plots, k is in units of m^{-1}, m is in units of $m^3 \, kg^{-1}$, $G_{diss}(k)$ is in W m kg^{-1} and $F_{diss}(m)$ is in W m^{-3}, so that both integrals give a power per unit mass.

dissipated power

$$P_{fs} = -7.9 \times 10^{-10} \text{ W kg}^{-1}. \tag{5.22}$$

These two predictions are in qualitative agreement, but with a difference of about an order of magnitude. (Had we used a factor of 4 in place of 3 in the definition of $m_\star$, (5.6), the fluxes would have to be multiplied by a factor of $(4/3)^{1+s} \simeq 1.5$, which does not affect the order of magnitude of the estimate. Here, we use the original choice of $m_\star$ from Cairns & Williams (1976) for simplicity. We hope to consider oceanographic implications of this choice in details in future publications.) We elucidate on possible reasons in the conclusions. Moreover, the following remarks are important for the sake of clarity.

Above, we have used the terminology dissipated power to indicate the amount of energy that is absorbed by the boundary sink at small scales. As far as the internal-wave kinetic equation is concerned, this sink is acting as an actual dissipation term. In the finescale parametrization picture to which we refer (see Polzin *et al.* 2014, § 2), this amount of energy is converted into turbulent kinetic energy at small scales, and therefore roughly equals the turbulent energy production. In turn, the latter contributes separately both to diapycnal mixing and to heat production, in proportions that can be quantified by closure assumptions beyond the scope of the present paper. We stress that the use of the word dissipation in this paper does not refer to dissipation of energy as heat, but to the role played by the sink that takes energy out of the wave system considered.

The energy fluxes at the boundaries, (5.12) and (5.13), show a non-trivial dependence on the variables k and m. In non-isotropic systems, rather than one single stationary state, it is common to have a family of stationary states (Nazarenko 2011, § 9.2.5) whose energy fluxes depend on k and m in different ways. The generalized KZ spectrum (that is the PR spectrum, for internal waves) is only one among the members of the family. Then, the locality conditions imply that for the internal waves only one solution is physically meaningful, i.e. $(a, b) = (3.69, 0)$. Indeed, since the solution is stationary,

for any enclosed region in $k - m$ space (contained in the inertial range where no sources or sinks are present), the incoming energy flux must be equal to the outgoing energy flux (and opposite in sign). Equivalently, as long as both ends of a boundary are fixed, the total outgoing flux through the boundary must be independent of the path of the boundary in $k - m$ space. For instance, one could show that the flux through the dissipative boundary equals the flux through the forcing boundary (respectively, the red and the black boundaries in figure 6).

Finally, we acknowledge the fact that the solutions with $b = 0$ are known in the literature as no flux solutions to the Fokker–Planck (diffusive) approximation to the kinetic equation (3.1). How this approximation is achieved is shown for instance in Lvov *et al.* (2010) by use of a straightforward leading-order approximation of the infrared ID interactions. An exact leading-order balance makes the infrared flux apparently vanish, whose trace in this paper is found in the two exact cancellations in the infrared region. However, our computations leading to (3.7) show how the next leading-order terms carry a small but non-zero flux toward high horizontal wavenumbers. Moreover, a net energy flux is indeed due to interactions outside the infrared region, such as the collinear interactions. Therefore, there is no mathematical contradiction in having $b = 0$ and a non-zero downscale energy flux. Indeed, the considerations in the present paper go way beyond the diffusive approximation to the internal-wave kinetic equation, where the concept of no flux solutions was concocted.

6. Discussion and conclusions

This paper is focused on the specific case of a scale-invariant field of internal waves in the ocean with vertically homogeneous ($b = 0$) wave action. For such a case we have found that

 (a) There necessarily exists a stationary state for $3 < a < 4$ dictated by the opposite signs of the infrared and ultraviolet resonant singularities;
 (b) The dominant contributions to the integrand of the kinetic equation are coming from ID and near-collinear resonances;
 (c) Both near-collinear and extreme scale-separated resonances are subject to subtractive cancellation between differing triad types;
 (d) Both types of resonances balance to zero for $a \simeq 3.69$ independently, cf. figure 4(*a*);
 (e) The contribution from the unclassified resonances is negligible, although it balances to zero at $a \simeq 3.69$, too;
 (f) We point out an important role played by collinear resonances, and we find a modified PR spectrum, (4.5), from a balance of the largest collinear contributions. Curiously, this solution is precisely in the middle of the interval of values of the exponent for which the collision integral is convergent (Zakharov *et al.* 1992). With the help of this analytical result, we explained how the exponent 3.69 appears concerning the near-collinear region. It is a result of a shift of the balance of the modified PR spectrum due to the negative contribution from the subleading collinear triads.
 (g) By considering the sign of the integrand of the kinetic equation we can visualize a downscale flux of energy in the horizontal wavenumber space, see figure 2.
 (h) Modifying the scale-invariant spectrum (3.9) to include natural physical boundaries in Fourier space, we numerically calculate the value of the spectral flux of energy towards high horizontal and vertical wavenumbers. This quantitative estimate might be useful for a direct estimate of turbulent energy mixing in the ocean.

(i) Our results compare favourably with the finescale parametrization formula of Polzin *et al.* (1995), being consistent within the range of an order of magnitude and reproducing similar scalings in the relevant parameters.

Our results are obtained for a scale-invariant internal-wave field with vertically homogeneous wave action profile. This profile is close to the scale-invariant limit of the GM spectrum, yet it is a strong idealization of the actual internal-wave spectrum. Generalizing the evaluations presented in this paper for more realistic ocean internal-wave spectra, including the presence of background rotation and spatial inhomogeneity, is a subject of current research.

Author ORCIDs.
- Giovanni Dematteis https://orcid.org/0000-0003-2918-8951;
- Yuri V. Lvov https://orcid.org/0000-0003-2153-4047.

REFERENCES

CAILLOL, P. & ZEITLIN, V. 2000 Kinetic equations and stationary energy spectra of weakly nonlinear internal gravity waves. *Dyn. Atmos. Oceans* **32** (2), 81–112.

CAIRNS, J.L. & WILLIAMS, G.O. 1976 Internal wave observations from a midwater float. *J. Geophys. Res.* **81**, 1943–150.

CHOI, Y., LVOV, Y.V. & NAZARENKO, S. 2004 Probability densities and preservation of randomness in wave turbulence. *Phys. Lett.* A **332**, 230–238.

CHOI, Y., LVOV, Y.V. & NAZARENKO, S. 2005 Joint statistics of amplitudes and phases in wave turbulence. *Physica* D **201**, 121–149.

DAVIS, G., JAMIN, T., DELEUZE, J., JOUBAUD, S. & DAUXOIS, T. 2020 Succession of resonances to achieve internal wave turbulence. *Phys. Rev. Lett.* **124** (20), 204502.

DEMATTEIS, G. & LVOV, Y. 2020 Downscale energy fluxes in scale invariant oceanic internal wave turbulence (supplementary materials). *J. Fluid Mech.* https://doi.org/10.1017/jfm.2021.99.

ERIKSEN, C.C. 1985 Some characteristics of internal gravity waves in the equatorial pacific. *J. Geophys. Res.* **90**, 7243–7255.

FERRARI, R. & WUNSCH, C. 2008 Ocean circulation kinetic energy: reservoirs, sources and sinks. *Ann. Rev. Fluid Mech.* **41**, 253–282.

GARRETT, C.J.R. & MUNK, W.H. 1972 Space-time scales of internal waves. *Geophys. Fluid Dyn.* **2**, 225–264.

GARRETT, C.J.R & MUNK, W.H. 1975 Space time scales of internal waves, progress report. *J. Geophys. Res.* **80**, 281–297.

GARRETT, C.J.R. & MUNK, W.H. 1979 Internal waves in the ocean. *Ann. Rev. Fluid Mech.* **11**, 339–369.

HASSELMANN, K 1966 Feynman diagrams and interaction rules of wave-wave scattering processes. *Rev. Geophys.* **4** (1), 1–32.

HEATH, M. 2002 *Scientific Computing*. McGraw-Hill.

HOLLOWAY, P., MÜLLER, G., HENYEY, F. & POMPHREY, N. 1986 Nonlinear interactions among internal gravity waves. *Rev. Geophys.* **24**, 493–536.

LIANG, C.-R., SHANG, X.-D., QI, Y.-F., CHEN, G.-Y. & YU, L.-H. 2018 Assessment of fine-scale parameterizations at low latitudes of the north Pacific. *Sci. Rep.* **8** (1), 1–10.

LVOV, Y.V., POLZIN, K.L. & TABAK, E.G. 2004 Energy spectra of the ocean's internal wave field: theory and observations. *Phys. Rev. Lett.* **92**, 128501.

LVOV, Y.V. & TABAK, E. 2001 Hamiltonian formalism and the Garrett-Munk spectrum of internal waves in the ocean. *Phys. Rev. Lett.* **87**, 168501.

LVOV, Y.V. & TABAK, E. 2004 A Hamiltonian formulation for long internal waves. *Physica* D **195**, 106.

LVOV, Y.V., TABAK, E., POLZIN, K.L. & YOKOYAMA, N. 2010 The oceanic internal wavefield: theory of scale invariant spectra. *J. Phys. Oceanogr.* **40**, 2605–2623.

LVOV, Y.V. & YOKOYAMA, N. 2009 Wave-wave interactions in stratified flows: direct numerical simulations. *Physica* D **238**, 803–815.

MACKINNON, J.A., *et al.* 2017 Climate process team on internal wave–driven ocean mixing. *Bull. Am. Meteorol. Soc.* **98** (11), 2429–2454.

MCCOMAS, C.H. & BRETHERTON, F.P. 1977 Resonant interaction of oceanic internal waves. *J. Geophys. Res.* **83**, 1397–1412.

MCCOMAS, C.H. & MÜLLER, P. 1981 The dynamic balance of internal waves. *J. Phys. Oceanogr.* **11**, 970–986.

MÜLLER, P., HOLLOWAY, G., HENYEY, F. & POMPHREY, N. 1986 Nonlinear interactions among internal gravity waves. *Rev. Geophys.* **24** (3), 493–536.

NAZARENKO, S. 2011 *Wave Turbulence*. Springer.

OLBERS, D.J. 1973 On the energy balance of small-scale internal waves in the deep sea. *Hamburg Geophys. Einzelschr.* **24**, 1–91.

OLBERS, D.J. 1976 Nonlinear energy transfer and the energy balance of the internal wavefield in the deep ocean. *J. Fluid Mech.* **74**, 375–399.

PAN, Y., ARBIC, B.K., NELSON, A.D., MENEMENLIS, D., PELTIER, W.R., XU, W. & LI, Y. 2020 Numerical investigation of mechanisms underlying oceanic internal gravity wave power-law spectra. *J. Phys. Oceanogr.* **50** (9), 2713–2733.

PELINOVSKY, E.N. & RAEVSKY, M.A. 1977 Weak turbulence of internal waves in the ocean. *Atmos. Ocean. Phys.* **13**, 187–193.

POLZIN, K. 2004 A heuristic description of internal wave dynamics. *J. Phys. Oceanogr.* **34** (1), 214–230.

POLZIN, K.L., GARABATO, A.C.N., HUUSSEN, T.N., SLOYAN, B.M. & WATERMAN, S. 2014 Finescale parameterizations of turbulent dissipation. *J. Geophys. Res.* **119** (2), 1383–1419.

POLZIN, K.L. & LVOV, Y.V. 2011 Toward regional characterizations of the oceanic internal wavefield. *Rev. Geophys.* **49**, RG4003.

POLZIN, K.L., TOOLE, J.M. & SCHMITT, R.W. 1995 Finescale parameterizations of turbulent dissipation. *J. Phys. Oceanogr.* **25** (3), 306–328.

VON STORCH, H. & HASSELMANN, K. 2010 Internal waves 1971–1981. In *Seventy Years of Exploration in Oceanography: A Prolonged Weekend Discussion with Walter Munk*, pp. 47–50. Springer.

VORONOVICH, A.G. 1979 Hamiltonian formalism for internal waves in the ocean. *Izv. Atmos. Ocean. Phys.* **15**, 52.

WHALEN, C.B., TALLEY, L.D. & MACKINNON, J.A. 2012 Spatial and temporal variability of global ocean mixing inferred from argo profiles. *Geophys. Res. Lett.* **39** (18).

WUNSCH, C. & WEBB, S. 1979 The climatology of deep ocean internal waves. *J. Phys. Oceanogr.* **9**, 235–243.

ZAKHAROV, V.E., L'VOV, V.S. & FALKOVICH, G. 1992 *Kolmogorov Spectra of Turbulence*. Springer.